Suspended carbon nanotube double quantum dots

A. K. Hüttel*, **B. Witkamp,** and **H. S. J. van der Zant**

Molecular Electronics and Devices, Kavli Institute of Nanoscience Delft, Delft University of Technology, PO Box 5046, 2600 GA Delft, The Netherlands

Received xx November 200x, revised xx November 200x, accepted xx December 200x
Published online xx December 200x

Key words carbon nanotube, double quantum dot, electron-phonon coupling
PACS 63.22.+m, 73.23.Hk, 73.63.Fg, 85.35.Kt

We present fabrication of and the first measurements on partially suspended double quantum dots in a carbon nanotube. Our objective is to enhance the energy resolution for spectroscopy of the vibronic modes of a suspended nanotube. When fabricating our devices, nanotubes grown on-chip are localized by AFM scanning, and subsequently contacted and gated with customized electrode geometries. First low-temperature transport measurement results are discussed, where the double quantum dot characteristics are clearly recognizable in measured current. In addition, we address current technological challenges and future plans.

Copyright line will be provided by the publisher

1 Introduction and motivation In present nano-electromechanical systems (NEMS) carbon nanotubes (CNT's) excel in a dual capacity. On one hand, their high tensile strength and aspect ratio make them ideal as molecular mechanical resonators [1, 2]. On the other hand, the extraordinary properties of carbon nanotubes as "one-dimensional molecular conductors" [3, 4] provide means of electronically accessing the mechanical properties in the quantum regime [5]. Previous experiments have shown [5] that vibronic excitations of CNT quantum dots can be resolved in transport measurements as sets of harmonic excited states at low energy. The energy scale of these states indicates that the longditudinal or stretching mode of the nanotubes was observed. The transversal or bending mode can more directly couple to the electric field between quantum dot and back gate charges, so a larger electron–phonon coupling is expected. The direct observation of this mode – with a corresponding energy scale of $\Delta\epsilon \lesssim 30\,\mu$eV at obtainable nanotube lengths $L \geq 90$ nm – in low-temperature transport measurements, however, provides a technological challenge.

One way to potentially increase the energy resolution in transport measurements is to use a double quantum dot (DQD) [6, 7] defined within the CNT as spectrometer. In bulk systems, this method has already been successfully used as detector of the phonon spectrum [8]. For a DQD with very weak tunnel coupling, the obtainable energy resolution can be limited by the tunnel rates between the quantum dots and the leads alone, independent of the electron temperature of the leads [6].

2 Fabrication methods The starting point of our fabrication is a bare SiO_2 on Si substrate with an oxide thickness of typically $0.5 - 1\,\mu$m. At first, e-beam and AFM alignment markers are defined by electron beam lithography. The AFM marker grid is designed such that it is possible to identify any position within the marker grid by looking at the shape of the four surrounding markers alone. Typically, for the e-beam alignment markers, a metallization of 5 nm titanium (as adhesion layer) and 60 nm platinum provides good contrast. As the marker shape is critical, $30 - 50$ nm chromium is used for the AFM marker grid because of its high thermal stability during the CNT growth. Subsequently a further electron beam

* Corresponding author: e-mail: a.k.huettel@tudelft.nl, Phone: +31 15 27 88102, Fax: +31 15 27 81413

lithography step is used to locally deposit catalyst for in-situ growth of the CNT's by chemical vapour deposition (CVD) [9].

After growth, the position of the CNT's is determined by atomic force microscopy (AFM). Using pattern recognition software, the resulting AFM scans are imported into a CAD system, such that the device geometries for subsequent electron beam lithography steps can be directly adapted to the position and angle of each CNT lying on the chip surface. Script-driven CAD processing is used to speed up the design process and "draw" device geometries with preselected dimensions (e.g. electrode width, separation between electrodes, ...) at the required coordinates.

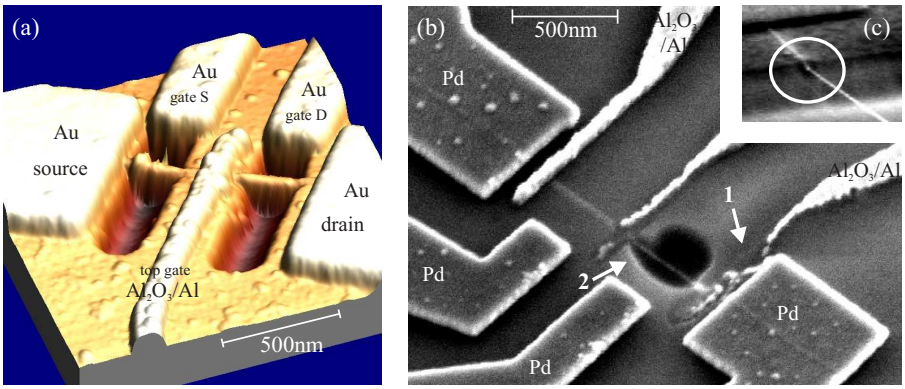

Fig. 1 Device geometries: (a) AFM picture of a carbon nanotube double quantum dot structure (underetched on both sides), with Cr/Au leads and a Al_2O_3/Al/AuPd central top gate. (b) SEM micrograph of a device underetched only on one side, with Ti/Pd contacts and three Al_2O_3/Al/AuPd top gates. This picture also serves to illustrate typical fabrication challenges (see text). (c) Detail of a SEM micrograph, showing a CNT pulled into the etched hole by surface tension during drying (see text).

Figure 1 displays two different approaches to fabricating a (partially) suspended DQD. In the device in the AFM picture of Fig. 1(a), the CNT is contacted with leads formed by a chromium adhesion layer below gold. This layer structure is known to lead typically to a highly resistive tunneling contact [10]. In previous work, this has been used to directly form a quantum dot between the contact electrodes [11]. In direct analogy, this effect is used here to define the tunnel barriers between the DQD and its leads. The central tunnel barrier between the two quantum dots forming the DQD is generated by local gating of the electrochemical potential. The required top gate is fabricated by first repeatedly evaporating a thin aluminum layer and oxidizing it in pure oxygen at atmospheric pressure, then covering this isolation oxide of ~ 5 nm thickness with aluminum and a gold palladium alloy [12].

Figure 1(b) displays a device using a complementary approach for the electrode geometry, more closely related to previous work on DQDs in carbon nanotubes [12]. Here, the contacts are formed by palladium on top of a thin titanium adhesion layer, which in turn generally leads to a low-resistance (Ohmic) contact between metal and CNT [13]. For defining the DQD potential structure, in this case three top gates (controlling the tunnel barriers source – dot 1, dot 1 – dot 2, and dot 2 – drain, respectively) are required. As a consequence, this geometry provides a higher level of control over the potential landscape.

For both device geometry variants, suspending the CNT is done by wet underetching in buffered HF. Care must be taken that the aluminum oxide / aluminum top gates do not come into contact with the etchant. For this purpose, in a further lithographic step the e-beam resist PMMA is used as etch mask [2]. After etching, the devices are soaked in warm isopropanole and placed wet onto a hot plate for drying.

3 First results Figure 2 displays exemplary measurements of partially functional structures. All data have been recorded in a dilution refrigerator setup at $T_{\mathrm{MC}} \lesssim 20$ mK and $T_{\mathrm{el}} \sim 100$ mK. In Fig. 2(a) and

© 2003 WILEY-VCH Verlag GmbH & Co. KGaA, Weinheim

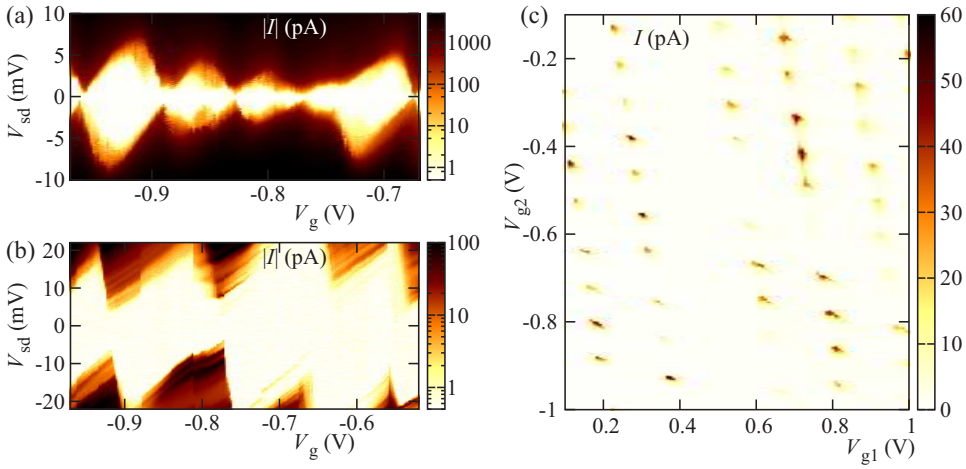

Fig. 2 Exemplary measurements of partially functional devices: (a), (b): Absolute value of the dc current through a DQD CNT structure similar to the one depicted in Fig. 1(a), as function of back gate voltage V_g and source-drain voltage V_{sd} for center top gate voltage (a) $V_{tg\text{-}c} = -1.2\,\mathrm{V}$ and (b) $V_{tg\text{-}c} = +1.2\,\mathrm{V}$. The gating effect towards a DQD potential structure for holes is recognizable. (c): dc-current through a DQD CNT structure similar to the one depicted in Fig. 1(b) as function of the two side gate voltages for a finite source-drain voltage $V_{sd} = 200\,\mu\mathrm{V}$.

(b), current through a device similar to the one of Fig. 1(a) is plotted as function of back gate voltage V_g and source-drain voltage V_{sd}. The central top gate voltage is chosen as (a) $V_{tg\text{-}c} = -1.2\,\mathrm{V}$ and (b) $V_{tg\text{-}c} = +1.2\,\mathrm{V}$. Whereas Fig. 2(a) displays nearly regular Coulomb blockade regions with a charging energy of up to $10\,\mathrm{meV}$ and broadened edges, in Fig. 2(b) a more than doubled charging energy of $\gtrsim 20\,\mathrm{meV}$, a large, highly irregular region of suppressed current around zero bias ($|V_{sd}| \lesssim 5\,\mathrm{mV}$) and sharp resonances of enhanced current at finite bias are observed. Comparing the two measurements, it becomes immediately clear that the nanotube is in the hole conduction regime and that in Fig. 2(b) for more positive gate voltage a central potential barrier is formed below the top gate. Misalignment of the chemical potentials in the two formed quantum dots leads to single electron tunneling suppression for a large bias region, alignment of ground and / or excited states to current maxima [6].

Figure 2(c) displays data taken from a different device, similar in design geometry to the one shown in Fig.1(b). The dc current at $V_{sd} = 0.2\,\mathrm{mV}$ is plotted as function of the applied voltage on the two side gates controlling the chemical potentials of the two quantum dots. In the parameter region shown, the characteristic stability diagram of a DQD at weak tunnel coupling can be immediately recognized [14]. The regions of Coulomb blockade and fixed electron number per quantum dot are rhomboids, indicating a very low capacitive coupling between the two quantum dots. At the triple points of the stability diagram where the electron number in both quantum dots can fluctuate [6, 7], discrete maxima of single electron tunneling current occur. Measurements at higher source-drain bias display the expected broadening of the triple points into triangular regions of finite current (data not shown).

4 Challenges and outlook DQD characteristics have been clearly observed in low-temperature transport measurements. Thus, there is a promising prospect of attaining a fully tunable weakly coupled DQD as spectrometer, and work on the respective chip structures is ongoing.

One important objective of our current work is improving the device fabrication yield. As can be observed in Fig. 1(b), the etch mask technique at the moment does not completely protect the aluminum oxide / aluminum top gates from the hydrofluoric acid (see e.g. arrow 1 in Fig. 1(b)). Judging from the shape of the etched holes, the etchant also flows along the CNT, enlarging the etched hole (see arrow 2).

© 2003 WILEY-VCH Verlag GmbH & Co. KGaA, Weinheim

An additional consistent feature is that the hydrofluoric acid attacks the oxide layer along the edges of aluminum oxide / aluminum gate contacts; no similar effect has been observed along chromium / gold or titanium / palladium contacts. Improvements towards decreasing edge roughness of the metal are required, as well as research into alternative top gate and isolator materials.

Imaging the devices fabricated up to now, further potential challenges can be identified. Surface tension during the drying process causes the CNT in many devices not to pass straight across the etched "hole" at the same level as the non-etched oxide surface. Instead the CNT follows the oxide surface for a small distance before stretching across at a lower height, as is illustrated in the detail SEM micrograph of Fig. 1(c). Effectively, several bends are introduced in the CNT on either side of the suspended length, potentially leading to tension and / or a local distortion of the band structure and barrier structures in transport. Currently tests using a critical point dryer are conducted in order to fully eliminate such surface tension effects.

Regarding the measurements, a common characteristic that has been observed several times in transport measurements has been a suppression of zero-bias current, as also shown in Fig. 2(a) (the "single-dot limit"). Although the observations are not fully conclusive up to now, it seems that this effect is also present in the DQD stability diagrams as e.g. Fig. 2(c) (data now shown), which rules out misalignment of the double quantum dot pseudo-potentials as a possible cause. Whether this is caused by additional potential barriers, as e.g. at the aforementioned bends of the CNT or growth / fabrication defects, or by phonon blockade effects [15] remains to be decided by additional measurements.

Acknowledgements Many thanks go to the Dutch organization for Fundamental Research on Matter (FOM), the NWO VICI program, and to the EC CANEL project (contract no. FP6-2004-IST-003673) for financial support. This publication reflects the views of the authors and not necessarily those of the EC. The Community is not liable for any use that may be made of the information contained herein.

References

[1] Sazonova, V. *et al.* *Nature* **431**, 284 (2004).
[2] Witkamp, B., Poot, M. & van der Zant, H. *Nano Letters* **6**, 2904 (2006).
[3] Oreg, Y., Byczuk, K. & Halperin, B. I. *Phys. Rev. Lett.* **85**, 365 (2000).
[4] Jarillo-Herrero, P., Sapmaz, S., Dekker, C., Kouwenhoven, L. P. & van der Zant, H. S. J. *Nature* **429**, 389 (2004).
[5] Sapmaz, S., Jarillo-Herrero, P., Blanter, Y. M., Dekker, C. & van der Zant, H. S. J. *Phys. Rev. Lett.* **96**, 026801 (2006).
[6] van der Wiel, W. G. *et al.* *Rev. Mod. Phys.* **75**, 1 (2002).
[7] Qin, H. *et al.* *phys. stat. sol. (c)* **1**, 2094 (2004).
[8] Fujisawa, T. *et al.* *Science* **282**, 932 (1998).
[9] Kong, J., Soh, H. T., Cassell, A. M., Quate, C. F. & Dai, H. *Nature* **395**, 878 (1998).
[10] Bockrath, M. *et al.* Single-Electron Transport in Ropes of Carbon Nanotubes. *Science* **275**, 1922 (1997).
[11] Sapmaz, S., Jarillo-Herrero, P., Kouwenhoven, L. P. & van der Zant, H. S. J. *Semic. Sci. Techn.* **21**, S52 (2006).
[12] Sapmaz, S., Meyer, C., Beliczynski, P., Jarillo-Herrero, P. & Kouwenhoven, L. *Nano Letters* **6**, 1350 (2006).
[13] Javey, A., Guo, J., Wang, Q., Lundstrom, M. & Dai, H. *Nature* **424**, 654 (2003).
[14] Hofmann, F. *et al.* *Phys. Rev. B* **51**, 13872 (1995).
[15] Braig, S. & Flensberg, K. *Phys. Rev. B* **68**, 205324 (2003).

© 2003 WILEY-VCH Verlag GmbH & Co. KGaA, Weinheim